Cerium oxide nanoparticles administration during machine perfusion of discarded human livers: A pilot study

Cerium oxide nanoparticles administration during machine perfusion of discarded human livers: a pilot study

Serena Del Turco[1*], Valentina Cappello[2], Christos Tapeinos[3], Aldo Moscardini[4], Laura Sabatino[1], Matteo Battaglini[3], Fabio Melandro[5], Francesco Torri[5], Caterina Martinelli[5], Serena Babboni[1], Beatrice Silvestrini[6], Riccardo Morganti[7], Mauro Gemmi[2], Paolo De Simone[5], Paulo N. Martins[8], Laura Crocetti[6], Adriano Peris[9], Giuseppina Basta[1], Gianni Ciofani[3] and Davide Ghinolfi[5*].

ORCID

Del Turco Serena 0000-0003-3722-8861

Ghinolfi Davide 0000-0001-7933-8941

Giuseppina Basta 0000-0003-0809-4374

Gianni Ciofani 0000-0003-1192-3647

Affiliations

[1]Institute of Clinical Physiology, CNR San Cataldo Research area, via Moruzzi 1, 56124 Pisa, Italy

[2]Center for Materials Interfaces, Electron Crystallography, Istituto Italiano di Tecnologia Viale Rinaldo Piaggio 34, Pontedera (PI), Italy 56025

[3]Smart Bio-Interfaces, Istituto Italiano di Tecnologia, Viale Rinaldo Piaggio 34, 56025 Pontedera (Pisa), Italy

[4]NEST, Scuola Normale Superiore, Piazza San Silvestro 12, 56127 Pisa, Italy

[5]Division of Hepatic Surgery and Liver Transplantation, University of Pisa Medical School Hospital, Via Paradisa 2, 56124 Pisa

[6]Division of Interventional Radiology, University of Pisa Medical School Hospital, Via Paradisa 2, 56124 Pisa

[7]Department of Statistics, University of Pisa, Pisa, Italy

[8]Department of Surgery, Division of Transplantation, University of Massachusetts, Worcester-MA, USA

[9]Regional Transplant Authority of Tuscany, Florence, Italy

Keywords: cerium oxide nanoparticles, machine perfusion, ischemia reperfusion injury, oxidative stress, liver transplantation, organ preservation

Abbreviations used (alphabetical order)

Alb-NC nanoceria conjugated with albumin; CAT catalase; Ce cerium; CIT cold ischemia time; EM electron microscopy; GM giant mitochondria; GSH glutathione; ICP-MS inductively coupled plasma-mass spectrometry; IL interleukin; IRI ischemia/reperfusion injury; LD lipid droplets; LT Liver Transplantation; MCP1 monocyte chemoattractant protein 1; MP machine perfusion; mtDNA mitochondrial DNA; NC nanoceria; NMP normothermic machine perfusion; NP nanoparticle; pLD peroxidized lipid droplets; ROS reactive oxygen species; SCS static cold storage; SOD superoxide dismutase; TEM transmission electron microscopy; TL telomere length

Grant and financial support

We are grateful to Mirko Prato of the Italian Institute of Technology in Genoa (Italy) for X-ray photoelectron spectroscopy experiments.

This study has been supported by a grant of the Regional Transplant Authority of Tuscany (Italy), OTT – Organizzazione Toscana Trapianti, Regional Act n.663/2015.

Conflict of interest

The authors of this manuscript have no conflict of interest to disclose.

Contact information

***Co-Corresponding Authors:**

Serena Del Turco, PhD

CNR, Institute of Clinical Physiology

San Cataldo Research Area

Via Moruzzi, 156124 Pisa, Italy

Phone: 0039-050-315 2661

Fax: 0039-050-315 2166

E-mail: serena@ifc.cnr.it

Davide Ghinolfi, MD, PhD

Division of Hepatic Surgery and Liver Transplantation

University of Pisa Medical School Hospital

Via Paradisa 2, 56124 Pisa, Italy

Phone: +39 050 995421

Fax: +39 050 995420

E-mail: d.ghinolfi@ao-pisa.toscana.it

https://orcid.org/0000-0003-3722-8861

Word count: 5324 words (including abstract, main text and references)

Number of tables: 1

Number of figures: 6

Abstract

The combined approach of *ex situ* normothermic machine perfusion (NMP) and nanotechnology represents a strategy to mitigate ischemia/reperfusion injury in liver transplantation. We evaluated the uptake, distribution, and efficacy of antioxidant cerium oxide nanoparticles (nanoceria) during normothermic perfusion of discarded human livers. Nine discarded human liver grafts were randomized in two groups and underwent 4 h NMP: five grafts were treated with nanoceria conjugated with albumin (Alb-NC; 50 μmol/L) and compared with four untreated grafts. The intracellular uptake of nanoceria was analyzed by electron microscopy and inductively coupled plasma-mass spectrometry (ICP-MS). The antioxidant activity of Alb-NC was assayed in liver biopsies by glutathione, superoxide dismutase and catalase assay, telomere length, and 4977-bp common mitochondrial DNA deletion ($mtDNA^{4977}$ deletion). Cytokine profile was evaluated in perfusate samples. Electron microscopy and ICP-MS confirmed Alb-NC internalization, rescue of mitochondrial phenotype, decrease of lipid droplet peroxidation, and lipofuscin granules in the treated grafts. Alb-NC exerted an antioxidant activity by increasing glutathione levels (%change: +94% ± 25%; $p = 0.01$), superoxide dismutase (+17% ± 4%; $p = 0.02$), and catalase activity (51% ± 23%; $p = 0.03$), reducing the occurrence of $mtDNA^{4977}$ deletion (-67.2% ± 11%; $p = 0.03$), but did not affect cytokine release. Alb-NC during *ex situ* perfusion decreased oxidative stress, up-regulating graft antioxidant defense. They could be a tool to improve quality graft during NMP and represent an antioxidant strategy aimed at protecting the graft against reperfusion injury during liver transplantation.

Introduction

Liver transplantation (LT) is subject to ischemia/reperfusion injury (IRI) during graft procurement, storage, implant, and the perioperative period. Severe IRI is associated with primary graft nonfunction, delayed function, and higher incidence of biliary complications such as ischemic-type biliary lesions.[1,2] Organ shortage in LT led to an increased use of extended criteria donors whose grafts are more vulnerable to IRI in comparison with standard grafts.[3,4] IRI is a multifactorial process that affect allograft function involving multiple hepatic cell types and processes as oxidative stress, mitochondrial damage, inflammation, microvascular dysfunction, cellular death, and immune activation.[5] Reactive oxygen species (ROS) are critical mediators in the early and late phases of hepatic IRI, and their excessive production results in an imbalance between oxidants and antioxidants that plays a role in cell death and liver damage.[6]

The transplant community needs to develop new approaches able to minimize IRI, thus optimizing liver utilization and improving outcome in LT recipients. Machine perfusion (MP) is a technology designed to protect organs from the detrimental effects of ischemia that occur during conventional static cold storage (SCS) and has the potential to act as a platform for direct release of therapeutic agents to organ, avoiding many of the limitations associated with off-target and systemic effects of drug administration in recipients. Normothermic MP (NMP) maintains normal metabolic conditions perfusing liver with oxygenated blood or other oxygen carriers and allows recovery and functional testing of graft before transplantation. Studies highlighted that NMP is associated with a significant reduction of organ discard rate[7,8] and reduced histological evidence of IRI in older organs.[5]

The combined approach of nanotechnology and MP represents a new era of therapeutic strategies designed to maximize long-term organ survival in LT. The use of appropriately modified nanoparticles (NPs) able to recognize the target organ and carry therapeutic agents gives advantages over systemic therapy, such as the use of lower dosages, localized and controlled drug delivery, and

reduced systemic side effects.[9,10] Cerium oxide NPs (nanoceria [NC]) have attracted great interest in different fields of medicine because of their regenerative, antioxidant, and anti-inflammatory properties. The coexistence of both $Ce^{3+/}Ce^{4+}$ ions in a stable form on their surface enables buffering of the ROS without being totally consumed, thus representing a long-term antioxidant if compared with the shorter half-life of classic antioxidants. The mixed valence state on the surface of NC is suggested to be responsible for mimicking the naturally occurring antioxidant enzymes such as superoxide dismutase (SOD)[11] and catalase (CAT)[11,12] and to scavenge peroxynitrite-derived radicals.[13] Many *in vitro* and *in vivo* studies demonstrated the hepatoprotective activity of NC.[14–19]

Our aim is to evaluate if NC administered during NMP can counteract the oxidative stress that characterizes IRI, providing graft protection before transplantation. Herein, we report the results of a prospective, randomized study to determine uptake, distribution, and efficacy of NC during NMP on discarded human livers.

Materials and Methods

Study design

Nine grafts deemed not suitable for clinical use were randomized into two groups: five were perfused in NMP in presence of NC conjugated with albumin (Alb-NC) (study group) and compared with four perfused untreated grafts (control group). All grafts underwent 4 h NMP. A bolus of Alb-NC was delivered into cardiotomy reservoir (final concentration of 50 μmol/L) immediately after NMP start. Liver and bile duct biopsies and perfusate samples were collected at the beginning (T0) and end (T1) of NMP. Perfusate samples of study group for ICP-mass analysis were collected at T0, after 120 min, and at T1 and, in 2 livers, were also collected after 30 and 60 min. The primary end point of the study was to compare antioxidant defenses between two groups (glutathione [GSH] levels, SOD, and CAT activity). The secondary end point was to evaluate (a) uptake and distribution of NC, (b) IRI as shown by ultrastructural damages at electron microscopy (EM; lipid droplets [LD], lipofuscin granules, mitochondrial pool) and DNA damages (telomere length [TL] and mtDNA4977 deletion), and (c)

changes in proinflammatory cytokine expression The protocol of this study conforms to the ethical guidelines of the 1975 Declaration of Helsinki and was approved by the local ethical committee (CEAVNO, protocol #13646).

Human livers procurement and evaluation.

Donors were evaluated as per our institutional clinical protocol. Organ procurements were performed using dual aortic and portal perfusion technique and liver biopsies performed based on surgeon's assessment.[20] Once deemed not suitable for clinical use at a national level, grafts were included in the study between December 2019 and January 2021, randomized by a third party with premade sealed envelopes, prepared at back table, and *ex situ* perfused at the facilities of the University of Pisa Medical School Hospital.

NMP setup description

The NMP setup and characteristics are described in the **Supporting Information**.

Synthesis and characterization of Alb-NC preparation

A detailed description of Alb-NC synthesis and characterization is provided in the **Supporting Information**.

Sample collection and processing

Liver biopsy samples were taken using a 14G Tru-cut and either stored in paraformaldehyde/glutaraldehyde solution for transmission EM (TEM) analysis or snap frozen in liquid nitrogen and stored at -80°C for further analysis. Frozen biopsies were cut in pieces, and liver tissue lysates were homogenized in tissue protein or DNA extraction buffer according to the protocols of different assays and centrifuged at 5,000 × *g* for 10 min at 4°C, and supernatants were stored at -80°C before use. The total protein content of liver homogenate supernatants was measured using bicinchoninic acid assay (Thermo Fisher Scientific). Perfusate samples (1.5 ml) were collected and centrifuged at 600*g* at 4°C for 10 min to remove cellular debris. The supernatant was frozen and stored at -80°C for subsequent analysis.

Ultrastructural analysis: TEM

Ultrastructural analysis was performed using TEM. Details of fixed and embedded samples sectioning, evaluation of LD peroxidation, and number and size of lipofuscin granules are reported in the **Supporting Information**.

Histological analysis of liver and bile duct biopsies

Histological analysis was performed as reported in **Supporting Information**.

Inductively coupled plasma-mass spectrometry analyses

To assess the liver uptake of Alb-NC during NMP, the amount of cerium (Ce), which is directly proportional to Alb-NC amount, was measured both in perfusate and in tissue biopsies, as described in the **Supporting Information**.

Biochemical assay of GSH levels, SOD and CAT activity

Reduced GSH levels were estimated by GSH colorimetric assay kit (BioVision Milpitas) following the manufacturer's protocol. Total activity of SOD (tot-SOD) isoenzymes, including copper/zinc SOD, manganese SOD, and extracellular SOD and CAT activity, were determined using a colorimetric kit following the manufacturer's protocol (Elabscience). GSH levels and SOD and CAT activity were normalized to total content protein, and the results were expressed as mean of percentage change as described in the statistical analysis.

Multiplex inflammatory cytokine array

Cytokines were measured in perfusate samples using Luminex xMAP Technology (Luminex Corporation). The target list included interferon-gamma, interleukin (IL)-1β, IL-6, IL-10, monocyte chemoattractant protein 1 (MCP1), and tumor necrosis factor alpha (TNF-α). Raw data were analyzed using MILLIPLEX Analyst 5.1 software (Millipore).

TL, mtDNA^{4977} deletion and flavin mononucleotide FMN measurement

Relative TL, mtDNA^{4977} deletion content and FMN measurement were assayed as described in the **Supporting Information**.

In vitro study

Human WRL-68 normal hepatocyte cell line was used to evaluate Alb-NC uptake and its effects in

the presence of oxidative stress. Cell culture, TEM analysis, cell viability, and ROS generation assay are described in the **Supporting Information**.

Statistical analysis it's impossible

to evaluate

A sample size of four liver grafts per group was required in order to evaluate a significant increase (from T = 0 to T = 1) between the study and control groups of the GSH levels equal to 5 (µg/mg total protein) (power 80%, α-error 5%, standard deviation equal to 2 µg/mg total protein). According to type of variables and level of distribution, descriptive statistics were reported as medians and interquartile ranges or as means ± SEM as appropriate unless otherwise indicated. The percentage change was calculated according to the following formula: ratio of (final value at T1 - initial value at T0)/(initial value at T0) × 100. We first evaluated the normality of each data distribution with Kolmogorov-Smirnov normality test, and then we used unpaired *t* test or Mann-Whitney nonparametric test to check the difference between control and study group. Paired *t* test or Wilcoxon nonparametric test was used to check the difference between T1 and T0 in each group. Agreement analysis between pre- and post-perfusion histology was performed by Cohen's test and comparisons between groups was carried out by chi square test or Fisher's exact test when appropriate. The data were analyzed using SPSS 21.0 (SPSS). A p value < 0.05 was considered significant.

Results

Donor demographics and perfusion parameters during NMP

Nine livers (eight donations after brain death, one donation after circulatory death grafts) were discarded based on histology evaluation. Reasons for discard were necrosis >10% (2 in each group), macrosteatosis >30% (1 in each group), or stage 3 fibrosis as per Ishak's classification (2 in the study group, 1 in the control). All grafts were successfully perfused with stable blood flows. Donors' characteristics stratified by group are shown in Table 1. Aspartate aminotransferase and alanine aminotransferase, lactate clearance, pH, and vascular flows variation during perfusion are shown in

the **Supporting Information** (**Figure S2A-F**). There were no significant differences among perfusion parameter, pH, or lactate clearance between the two groups. A lower transaminases trend was noted in the control groups.

Characterization of Alb-NC

The combination of NC and albumin results in irregular conjugates in terms of size and morphology (**Figure S3A,B**). Aggregation of NC in neutral conditions (Dulbecco's phosphate-buffered saline pH 7.4) results in stable conjugates (average size of 196 ± 5.8 nm, stable up to more than 25 days) as shown from the dynamic light scattering data (**Figure S3C**). The acquired XPS spectrum is consistent with a Ce(III) concentration of 69% ± 2% and a Ce(IV) concentration of 31% ± 2%, corresponding to a Ce(III)/Ce(IV) ratio of ~2.2 showing the antioxidant properties of the NC conjugates (**Figure S3D**).

Alb-NC uptake and distribution in human liver

After 4 h NMP, liver biopsies showed internalization of Alb-NC at different levels (**Figure 1**): in the vascular system (**Figure 1a**), in the endothelial cells surrounding single vessel, and in the hepatocytes (**Figure 1b**). We observed that Alb-NC cross endothelial cells by transcytosis (**Figure 1b**) without any side effects on these cells. Small cytosolic aggregates and isolated NPs were visible inside hepatocytes (**Figure 1b**). Alb-NC were stored inside mitochondria (**Figure 1c**) and in the endosomal compartment (**Figure 1e–g**). The presence of isolated NPs is shown in forming endosomes (**Figure 1e**) and early endosomes (**Figure 1f**), and the presence of aggregated and isolated NPs is observed in late endosomes (**Figure 1g**). Alb-NC were also stored in lipofuscin granules (**Figure 1d**) that might constitute both a degradation pathway for Alb-NC excretion and a site of detoxification of nondegradable oxidized products by Alb-NC.

Liver internalization of Alb-NC during NMP was confirmed by the increased content of Ce in liver tissues after 2 h perfusion evaluated by inductively coupled plasma-mass spectrometry (**Figure 2A**) At the same time, Ce content in perfusates decreased during NMP, and an 81-fold decrease of Ce was noted at 2 h (**Figure 2B**). Perfusate of the two study group livers with additional samples analyses

showed a 56, 74, 86, and 89-fold decrease at 30, 60, 120, and 240 min, respectively.

LD. **Figure 3A** shows representative EM images of liver biopsies both of control (**Figure 3Aa,b**) and study group (**Figure 3Ac,d**) at T0 and T1. In the control group, the percentage of peroxidized LD (pLD) increased from T0 to T1 (T0: 68.2% ± 27.7% vs. T1: 81.2% ± 18.1%; $p = 0.12$), whereas pLD decreased significantly at T1 in the study group (T0: 38.2% ± 24.3% vs. T1: 112% ± 8.4%; $p < 0.001$) (**Figure 3B**).

Lipofuscin granules. **Figure 4A** shows EM images of liver biopsies both of control (**Figure 4Aa,b**) and study group (**Figure 4Ac,d**) at T0 and T1. Lipofuscin granules are outlined in black boxes. The morphometric evaluation of lipofuscin granules area in the control group showed a significant increase of averaged area (T0: 2.9± 2.5 vs. T1: 4.2 ± 5.1; $p = 0.048$), whereas their number did not change at T1 respect to T0 (T0: 0.009 ± 0.0045 vs. T1: 0.008 ± 0.003; $p = 0.23$) (**Figure 4B,C**). Conversely, in the study group, we observed a comparable reduction of number (T0: 0.007 ± 0.0015 vs. T1: 0.0045 ± 0.002; $p = 0.01$) and mean area of granules at T1 (T0: 2.8 ± 3 vs. T1: 1.2 ± 1.4; $p < 0.001$) (**Figure 4B,C**). Baseline values of the number and average area of granules did not differ between two groups at T0 ($p = 0.06$ and $p = 0.05$, respectively), whereas they are lower in the study group than the control group at T1 ($p = 0.01$ and $p < 0.001$, respectively).

Mitochondrial pool. We observed morphological alterations of mitochondrial pool as swelling, alteration of matrix (**Figure S4a,d,g**, white boxes) and cristae (**Figure S4d,g**), and the presence of giant mitochondria (GM) (**Figure S4d**) in each analyzed sample at T0. In the control group, we observed the presence of GM and variation of mitochondrial matrix after NMP (**Figure S4b,c**), whereas size and cristae organization of mitochondria did not differ from T0. In the study group instead, we observed a rescue of mitochondrial morphology compared with T0 with a better cristae organization (**Figure S4e,f,h,i**) and a reduced presence of GM compared with T0. For the evaluation of this morphological baseline, we also compared mitochondrial pool of the hepatocytes in liver biopsies with those observed in an *in vitro* model of oxidative stress induced by H_2O_2 in WRL-68 human hepatocyte line. Alb-NC did not affect cell viability, reduced oxidative stress in WRL-68, and

rescued mitochondrial phenotype in WRL-68 cell line (**Figure S5A,B,C**).

Liver biopsies and bile duct histology analysis are reported in **Table S1 and Table S2**. No substantial differences at the end of perfusion were noted in both groups, as demonstrated by an acceptable agreement measured with Cohen's kappa/percentages **(Table S1-S2)**. Moreover, no differences were noted between two groups at T1 (**Table S3**).

ROS scavenging activity of Alb-NC

Figure 5 shows the variation of GSH concentration and SOD and CAT activity in liver biopsies of control and study group. Our results demonstrated that livers of the study group showed increased levels of GSH and SOD and CAT activity compared the control group (GSH% change: 94% ± 25% vs. -13.4 ± 4.2, $p = 0.01$; SOD% change: 17% ± 3.9%, vs. -17% ± 7.2%, $p = 0.02$; CAT% change: 51% ± 23% vs. -37% ± 20%, $p = 0.03$).

Cytokine profiling

In both groups, we observed an increase of all cytokines and MCP1 after NMP. No significant differences in fold change of cytokines were noted between groups. Interestingly, the fold change of cytokines in the study group tends to be lower compared with those in the control group. A greater fold change increase of anti-inflammatory IL-10 has been observed in the perfusate of study group compared with control group (**Figure S6**).

Detection of the relative mtDNA^{4977} and TL in liver biopsies and FMN measurement in perfusates

The relative quantification of mtDNA^{4977} deletion expression decreased significantly after NMP in study group compared with control group (%change: -67.2% ± 11% vs. 83.5% ± 73%; respectively, $p = 0.03$) (**Figure 6A**). Conversely, TL (expressed as T/S ratio) was not significantly different between two groups (19.2% ± 13.6% vs. 6.6% ± 14%; respectively, $p = 0.57$) (**Figure 6B**).

FMN-related fluorescence increased both in control and study group after 4 h of perfusion, but no differences in FMN increase were detected between study and control group after reperfusion (%change: 223±114 (n=3) vs. 119±40; respectively p=0.45).

Discussion

The present randomized study proves that NMP can be used as platform to deliver NPs to human livers. Alb-NC administered during NMP exert an antioxidant activity and increase antioxidant defenses in human livers, thus suggesting a potential for IRI minimization.

IRI following LT remains a major problem in clinical practice because of its association with increased risk of organ failure and post-LT complications.[2] Several approaches to mitigate IRI have been the subject of intense investigation. NMP is a dynamic preservation approach that offers the opportunity to resuscitate grafts by repairing cell injury, assess organ viability before implantation,[5,8,21,22] and test new pharmacological approaches by direct delivery to a functioning organ, reducing adverse effects related to systemic therapy.[10,23–25] The antioxidant therapy in LT could be a potentially attractive strategy to counteract IRI-induced oxidative stress.[26] One of the advantages of NC application is the permanent activity due to their regenerative/autocatalytic properties that allows them to work at lower doses and does not require a continuous application like other antioxidant therapies.[27]

Our study demonstrates hepatic internalization of Alb-NC, confirming that NMP is an optimal platform for organ treatment. Moreover, hepatocytes positive for Alb-NC internalization showed a rescued architecture at TEM analysis, suggesting that cell vitality was not affected. EM showed that Alb-NC crossed the endothelium into hepatocytes and are stored in mitochondria, early and late endosomes, and lipofuscin granules. The increase of Ce in liver grafts parallel a decrease of Ce in the perfusate and suggests an efficient uptake of NPs. The uptake of Alb-NC would start within the initial 30 min and peak at 2 h, remaining fairly constant during NMP, suggesting that an *ex situ* perfusion limited to 2 h might be enough for drug delivery purposes. The demonstration that transcytosis is responsible for Alb-NC uptake is of great importance, as this mechanism is not affected by anoxia or temperature but influenced by hydrostatic pressures,[28] suggesting that even hypothermic-MP could have the potential to deliver NPs[29] and provide the hepatocytes of antioxidant agents before revascularization.

We analyzed three different cellular compartments that may be affected by hepatic IRI: 1) LD, 2) lipofuscin granules, and 3) mitochondrial pool. LD's main function is storing and providing energy and preventing lipotoxicity and oxidative stress.[30,31] In pathological conditions, LD are both a target of oxidative stress-mediated peroxidation and the substrate of phagosomes-mediated lipolysis as well.[30] Our findings demonstrated a decreased number of pLD after perfusion in presence of NC compared with perfusion alone.

Lipofuscin granules are lysosomes-derived structures present in cells with a high lipid metabolism and represent a storage of nondegradable oxidation products arising from aging and oxidative damage. We found decreased number and mean area of granules in the study group after NMP, as morphological expression of NC-protective activity on oxidative-induced cellular damage. The increased mean area of lipofuscin granules in the control group could be attributed to the enlargement of granules due to the accumulation of peroxidized material induced by the fusion of small granules observed at T0 in the large structures measured at T1. It might be postulated that the presence of Alb-NC in lipofuscin granules could constitute both a degradation pathway for Alb-NC excretion or a site of detoxification of nondegradable oxidized products of Alb-NC.

Restoration and maintenance of mitochondrial function after SCS should be considered a main strategy for graft preservation.[32] Mitochondria are the main source of ROS and are particularly vulnerable to oxidative injury.[33,34] Mitochondrial damage may impair the electron flow and promote the mitochondrial Ca^{2+} flux and ROS production that damage mitochondrial membrane lipids, increasing mitochondrial membrane permeability along with Ca^{2+}-induced mitochondrial swelling.[32] EM-based ultrastructural analysis demonstrated mitochondrial swelling with alterations of mitochondrial matrix and cristae and the presence of GM in SCS-preserved livers. GM are peculiarly shaped, extremely large mitochondria in hepatic parenchymal cells, whose presence is linked with the oxidative stress following the IRI.[35] After NMP, control group livers did not show changes in mitochondrial phenotype. In the study group instead, we observed a rescue of mitochondrial morphology after NMP, a better cristae organization and reduced GM number. Because

mitochondrial function is intrinsically linked to normal ultrastructure,[36,37] we may also speculate that a better organization of cristae is associated with a rescue of mitochondrial functionality. The ability of NC to preserve mitochondrial morphology and function under powerful oxidative insults has been already demonstrated in skin fibroblasts exposed to pro-oxidative insults.[38] Our *in vitro* results on WRL-68 cells support this evidence. In fact, Alb-NC were able to improve mitochondrial morphology in oxidative-induced damage, reducing ROS generation.

ROS in cells are neutralized by antioxidant defense system including SOD, CAT, and GSH.[39] Under homeostatic conditions, liver has high levels of antioxidants effective at combating the damaging effects of ROS.[39] However, upon reperfusion of ischemic livers, elevated levels of ROS overwhelm the hepatic antioxidant system leading to oxidative stress.[40] Agents that enhance or mimic the activity of these defenses are the principal strategies underlying antioxidant therapy. It has been well established that NC counteract ROS accumulation and increase antioxidant defenses exhibiting SOD and CAT mimetic activity[11,12] and hydroxyl radical scavenging activity[41] in conditions of oxidative stress. In the present work, we found increased levels of GSH in the study group after NMP. GSH is the main intracellular redox scavenger of the liver, whose depletion causes oxidative stress. GSH also serve as a cofactor in many enzymatic reactions that involve GSH-dependent enzyme.[42] We demonstrated that NC replaced SOD and CAT activity in liver biopsies, increasing the antioxidant defenses during NMP. Moreover, NC already present in the liver, thanks to intrinsic antioxidant enzyme mimetic activity, would also ensure ROS scavenging activity during the later reperfusion phase of LT.

Increasing levels of inflammatory cytokines in perfusate have been shown during liver NMP, which may reflect IRI-mediated inflammation.[5,43,44] The cytokine profile showed increased fold change of cytokine release in perfusate of both groups, but the anti-inflammatory IL-10, involved in the reduction of damage-associated IRI inflammation,[45] tended to be higher in the study group than the control group. The mechanisms among which ROS may favor cytokine release include the control of release mechanisms from cytosol or gene expression.[46] Enhanced liver antioxidant defenses, as after

liver uptake of Alb-NC, might affect cytokine release from cytosol and, at the same time, their tissue gene expression. However, effects of Alb-NC on tissue gene expression of cytokines is not evaluable, measuring the cytokine release after 4 h NMP.

Given the strict correlation between oxidative stress and DNA damage, we evaluated the potential of NC to counteract two of the main events associated with genomic and mitochondrial DNA (mtDNA) damage: telomere attrition and mtDNA^{4977} deletion. In normal livers, telomere shortening is a natural process associated with hepatocytes aging. However, in pathological conditions, marked telomere attrition induced by external factors, such as oxidative stress or repeated antigen exposure, is recognized as DNA damage and cellular protective mechanisms driving to cell cycle arrest and apoptosis.[47] Among mtDNA deletions, the mtDNA^{4977} deletion provokes a relevant destruction of one third of mitochondrial genome and has been reported in several forms of diseases and in aging. In particular, it causes an important failure of adenosine triphosphate production and subsequently impairs mitochondrial oxidative phosphorylation, the main cellular energy-productive process. The mtDNA^{4977} deletion and marked increase of ROS have been reported in patients with hepatocellular carcinoma, and may play a pivotal role in the pathogenesis of the disease.[48] Our results demonstrated that mtDNA^{4977} deletion content decreased significantly after NMP in the study group, suggesting that the presence of Alb-NC in mitochondria, as evidenced by TEM analysis, counteracts mitochondrial oxidative stress and decreases mtDNA damage. Conversely to results previously obtained in human endothelial cells, where NC were able to counteract the oxidative-induced telomere shortening,[49] we did not observe a significative reduction of telomere shortening in the study group.

The reperfusion of ischemic tissue leads to FMN dissociation from complex I, resulting in a decline of mitochondrial C-1 activity, and to ROS generation at multiple sites in the mitochondria. FMN has been proposed as a marker of mitochondrial dysfunction and predictive marker for early allograft dysfunction when measured during hypothermic oxygenated liver perfusion.[50] On the other hand, no data exist about FMN release during NMP of human livers. Here, we demonstrated not differences in

FMN-related fluorescence in perfusates of study and control group after reperfusion, suggesting that normothermic perfusion may induce FMN release from discarded human livers independently from NC administration.

Our study presents some obvious limitations. First, the reduced number of discarded human livers in clinical practice do not allow for the enrollment of large series of grafts and influence the heterogeneity of liver characteristics in the two groups, which can only be minimized by randomization. Second, the mandatory offer of the grafts to all Italian transplant centers before being deemed unsuitable for transplant had a relevant impact on the prolonged cold ischemia time (CIT) before NMP can be commenced. The possibility of using good quality graft with limited CIT would have increased the rate of bile producing grafts, thus allowing a better evaluation of Alb-NC efficacy and excretion. Third, we do not have information on NC uptake and efficacy when different Alb-NC concentrations or different types of *ex situ* perfusion (hypothermic or subnormothermic) are used. In addition, the long-term effects and final fate of Alb-NC after NMP are not still known and need to be explored in future works.

Although the reported limitations must be kept in consideration for a critical evaluation of this work, we believe the results obtained by this pilot study are encouraging to provide valuable insights for future experimental studies and to lay the foundation for the use of nanotechnologies in transplant clinical practice.

Supporting Information

Additional supporting information may be found online in the **Supporting Information**.

References

1. Guichelaar MMJ, Benson JT, Malinchoc M, Krom RAF, Wiesner RH, Charlton MR. Risk factors for and clinical course of non-anastomotic biliary strictures after liver transplantation. *Am J Transplant.* 2003;3(7):885–890.
2. Zhai Y, Petrowsky H, Hong JC, Busuttil RW, Kupiec-Weglinski JW. Ischaemia-reperfusion injury in liver transplantation--from bench to bedside. *Nat Rev Gastroenterol Hepatol.* 2013;10(2):79–89.
3. Busquets J, Xiol X, Figueras J, et al. The impact of donor age on liver transplantation: influence of donor age on early liver function and on subsequent patient and graft survival. *Transplantation*

2001;71(12):1765–1771.
4. Dasari BV, Mergental H, Isaac JR, Muiesan P, Mirza DF, Perera T. Systematic review and meta-analysis of liver transplantation using grafts from deceased donors aged over 70 years. *Clin Transplant.* 2017;31(12):e1319.
5. Ghinolfi D, Rreka E, De Tata V, et al. Pilot, open, randomized, prospective trial for normothermic machine perfusion evaluation in liver transplantation from older donors. *Liver Transpl.* 2019;25(3):436–449.
6. Yao W, Tai LW, Liu Y, Hei Z, Li H. Oxidative stress and inflammation interaction in ischemia reperfusion injury: role of programmed cell death. *Oxid Med Cell Longev.* 2019;2019:6780816.
7. Ravikumar R, Jassem W, Mergental H, et al. Liver transplantation after *ex vivo* normothermic machine preservation: a phase 1 (first-in-man) clinical trial. *Am J Transplant.* 2016;16(6):1779–1787.
8. Nasralla D, Coussios CC, Mergental H, et al., for the Consortium for Organ Preservation in Europe. a randomized trial of normothermic preservation in liver transplantation. *Nature* 2018;557(7703):50–56.
9. Yetisgin AA, Cetinel S, Zuvin M, Kosar A, Kutlu O. Therapeutic nanoparticles and their targeted delivery applications. *Molecules* 2020;25(9):2193.
10. Ghinolfi D, Melandro F, Torri F, et al. Extended criteria grafts and emerging therapeutics strategy in liver transplantation. The unstable balance between damage and repair. *Transplant Rev.* 2021;35(4):100639.
11. Heckert EG, Karakoti AS, Seal S, Self WT. The role of cerium redox state in the SOD mimetic activity of nanoceria. *Biomaterials* 2008;29(18):2705–2709.
12. Pirmohamed T, Dowding JM, Singh S, et al. Nanoceria exhibit redox state-dependent catalase mimetic activity. *Chem Commun (Camb).* 2010;46(16):2736–2738.
13. Dowding JM, Dosani T, Kumar A, Seal S, Self WT. Cerium oxide nanoparticles scavenge nitric oxide radical (˙NO). *Chem Commun.* 2012;48(40):4896–4898.
14. Oró D, Yudina T, Fernández-Varo G, et al. Cerium oxide nanoparticles reduce steatosis, portal hypertension and display anti-inflammatory properties in rats with liver fibrosis. *J Hepatol.* 2016;64(3):691–698.
15. Carvajal S, Perramón M, Oró D, et al. Cerium oxide nanoparticles display antilipogenic effect in rats with non-alcoholic fatty liver disease. *Sci Rep.* 2019;9(1):12848.
16. Córdoba-Jover B, Arce-Cerezo A, Ribera J, et al. Cerium oxide nanoparticles improve liver regeneration after acetaminophen-induced liver injury and partial hepatectomy in rats. *J Nanobiotechnology* 2019;17(1):112.
17. Ni D, Wei H, Chen W, et al. Ceria nanoparticles meet hepatic ischemia-reperfusion injury: the perfect imperfection. *Adv Mater.* 2019;31(40):e1902956.
18. Adebayo OA, Akinloye O, Adaramoye OA. Cerium oxide nanoparticles attenuate oxidative stress and inflammation in the liver of diethylnitrosamine-treated mice. *Biol Trace Elem Res.* 2020;193(1):214–225.
19. Fernández-Varo G, Perramón M, Carvajal S, et al. Bespoken nanoceria: an effective treatment in experimental hepatocellular carcinoma. *Hepatology* 2020;72(4):1267–1282.
20. Ghinolfi D, Tincani G, Rreka E, et al. Dual aortic and portal perfusion at procurement prevents ischaemic-type biliary lesions in liver transplantation when using octogenarian donors: a retrospective cohort study. *Transpl Int.* 2019;32(2):193–205.
21. Watson CJE, Kosmoliaptsis V, Pley C, et al. Observations on the ex situ perfusion of livers for transplantation. *Am J Transplant.* 2018;18(8):2005–2020.
22. Detelich DJF, Markmann JF. The dawn of liver perfusion machines. *Curr Opin Organ Transplant.* 2018;23:151–161.
23. Xu J, Buchwald JE, Martins PN. Review of current machine perfusion therapeutics for organ preservation. *Transplantation.* 2020;104(9):1792–1803.
24. DiRito JR, Hosgood SA, Tietjen GT, Nicholson ML. The future of marginal kidney repair in the context of normothermic machine perfusion. *Am J Transplant.* 2018;18(10):2400–2408.

25. Tietjen GT, Hosgood SA, DiRito J, et al. Nanoparticle targeting to the endothelium during normothermic machine perfusion of human kidneys. *Sci Transl Med.* 2017;9(418):eaam6764.
26. Weigand MA, Plachky J, Thies JC, et al. N-acetylcysteine attenuates the increase in alpha-glutathione S-transferase and circulating ICAM-1 and VCAM-1 after reperfusion in humans undergoing liver transplantation. *Transplantation.* 2001;72(4):694–698.
27. Casals E, Zeng M, Parra-Robert M, et al. Cerium oxide nanoparticles: advances in biodistribution, toxicity, and preclinical exploration. *Small* 2020;16(20):1907322.
28. Predescu SA, Predescu DN, Malik AB. Molecular determinants of endothelial transcytosis and their role in endothelial permeability. *Am J Physiol Lung Cell Mol Physiol.* 2007;293(4):L823–L842.
29. Gillooly AR, Perry J, Martins PN. First report of siRNA uptake (for RNA interference) during *ex vivo* hypothermic and normothermic liver machine perfusion. *Transplantation.* 2019;103(3):e56–e57.
30. Suzuki M, Shinohara Y, Ohsaki Y, Fujimoto T. Lipid droplets: size matters. *J Electron Microsc (Tokyo).* 2011;60 Suppl 1:S101–S116.
31. Henne WM, Reese ML, Goodman JM. The assembly of lipid droplets and their roles in challenged cells. *EMBO J.* 2018;37(27):e98947.
32. Horváth T, Jász DK, Baráth B, Poles MZ, Boros M, Hartmann P. Mitochondrial consequences of organ preservation techniques during liver transplantation. *Int J Mol Sci.* 2021;22(6):2816.
33. Chouchani ET, Pell VR, James AM, et al. A unifying mechanism for mitochondrial superoxide production during ischemia-reperfusion injury. *Cell Metab.* 2016;23(2):254–263.
34. Mailloux RJ. An update on mitochondrial reactive oxygen species production. *Antioxidants (Basel).* 2020;9(6):472.
35. Shami GJ, Cheng D, Verhaegh P, Koek G, Wisse E, Braet F. Three-dimensional ultrastructure of giant mitochondria in human non-alcoholic fatty liver disease. *Sci Rep.* 2021;11(1):3319.
36. Cogliati S, Frezza C, Soriano ME, et al. Mitochondrial cristae shape determines respiratory chain supercomplexes assembly and respiratory efficiency. *Cell* 2013;155(1):160–171.
37. Quintana-Cabrera R, Mehrotra A, Rigoni G, Soriano ME. Who and how in the regulation of mitochondrial cristae shape and function. *Biochem Biophys Res Commun.* 2018;500(1):94–101.
38. Pezzini I, Marino A, Del Turco S, et al. Cerium oxide nanoparticles: the regenerative redox machine in bioenergetic imbalance. *Nanomedicine (Lond).* 2017;12(4):403–416.
39. Li S, Tan HY, Wang N, et al. The role of oxidative stress and antioxidants in liver diseases. *Int J Mol Sci.* 2015;16(11):26087–26124.
40. Akhtar MZ, Henderson T, Sutherland A, Vogel T, Friend PJ. Novel approaches to preventing ischemia-reperfusion injury during liver transplantation. *Transplant Proc.* 2013;45(6):2083–2092.
41. Xue Y, Luan Q, Yang D, Yao X, Zhou K. Direct evidence for hydroxyl radical scavenging activity of cerium oxide nanoparticles. *J Phys Chem C.* 2011;115(11):4433–4438.
42. Marí M, de Gregorio E, de Dios C, et al. Mitochondrial glutathione: recent insights and role in disease. *Antioxidants (Basel)* 2020;9(10):909.
43. Chae MS, Kim Y, Chung HS, et al. Predictive role of serum cytokine profiles in acute kidney injury after living donor liver transplantation. *Mediators Inflamm.* 2018;2018:8256193.
44. Ghinolfi D, Dondossola D, Rreka E, et al. Sequential use of normothermic regional and ex situ machine perfusion in donation after circulatory death liver transplant. *Liver Transpl*. 2021;27(3):385–402.
45. Yoshidome H, Kato A, Edwards MJ, Lentsch AB. Interleukin-10 suppresses hepatic ischemia/reperfusion injury in mice: implications of a central role for nuclear factor kappaB. *Hepatology* 1999;30(1):203–208.
46. Checa J, Aran JM. Reactive oxygen species: drivers of physiological and pathological processes. *J Inflamm Res.* 2020;13:1057–1073.
47. Barnard A, Moch A, Saab S. Relationship between telomere maintenance and liver disease. *Gut Liver.* 2019;13(1):11–15.
48. Guo ZS, Jin CL, Yao ZJ, Wang YM, Xu BT. Analysis of the mitochondrial 4977 bp deletion in patients with hepatocellular carcinoma. Balkan J Med Genet. 2017;20(1):81–86.

49. Del Turco S, Ciofani G, Cappello V, et al. Effects of cerium oxide nanoparticles on hemostasis: coagulation, platelets, and vascular endothelial cells. J Biomed Mater Res A. 2019;107(7):1551–1562.
50. Schlegel, A, Xavier M, Mueller M, et al. Hypothermic oxygenated perfusion protects from mitochondrial injury before liver transplantation. EBioMedicine. 2020 Oct;60:103014.

Legends to Figures

Figure 1. Uptake and distribution of Alb-NC in human liver after 4 h of NMP. EM micrograph of the vessel structure with Alb-NC (a). Alb-NC moving from the vessel lumen, trough endothelial cell (EC) by transcytosis, to neighboring hepatocytes (HP) (b). Aggregates (§) or isolated (arrowheads) Alb-NC stored inside hepatocyte mitochondria (c), forming endosome (e), early endosome (f), and late endosome (g). Lipofuscin granules positive to Alb-NC (d).

Figure 2. Inductively coupled plasma-mass spectrometry (ICP-MS) analysis of Ce content in perfusate (A) and liver biopsies (B). Data are expressed as mean ± SD. *p = 0.01; **p = 0.02; ***p = 0.02; ****p < 0.001vs. 0 min.

Figure 3. (A) Representative low magnification (LM) TEM images of human liver biopsies before (T0) and after (T1) 4 h of NMP in the control (a,b) and study groups (c,d). White boxed regions are characterized by normal LD, whereas black boxed regions are characterized by peroxidized ones. The pLD are characterized by a pale halo between membrane and lipid content as described in the Materials and Methods. (B) Quantitative analysis of the percentage of peroxidized LD observed in each LM image analyzed. *p < 0.001 vs. control group at T1; **p < 0.001 vs. T0.

Figure 4. (A) Representative low mag (LM) TEM images of human liver biopsies before (T0) and after (T1) 4 h of NMP in the control (a,b) and study groups (c,d). Boxed areas in all images represent example lipofuscin granules. (B) Quantitative analysis of the number of lipofuscin granules normalized for the area of hepatocytes. Data are shown as mean ± SD. *p = 0.011 vs. T0; **p = 0.0098 vs. control group. (C) Quantitative analysis of the average area of lipofuscin granules. Data are shown as mean ± SD. ***p = 0.048 vs. T0; ****p < 0.001 vs. control group at T1.

Figure 5. The percentage change of GSH levels and tot-SOD and CAT activity in tissue homogenates of control and study group compared with T0. Data are shown as the mean value of percentage change ± SEM. *p = 0.01; **p = 0.02; ***p = 0.03 vs. control group.

Figure 6. The percentage change of relative fluorescence of mtDNA^{4977} and T/S ratio in liver biopsies of both groups compared with T0. Data are shown as the mean value of percentage change ± SEM. Number of observations: mtDNA^{4977} = 4, T/S = 5 in the study group; mtDNA^{4977} = 3, T/S = 3 in the control groups. *p = 0.03 vs. control group.

Table 1. Donors' characteristics

	Study Group (*n* = 5)	Control Group (*n* = 4)	*p*
Age (years)	75 (63-77)	86 (79-88)	0.207
Sex (M/F)	1/4 (20/80)	0/4 (0/100)	0.343
BMI (n)	25 (24-28)	26 (23-29)	0.621
ICU stay (days)	2 (1-5)	1 (1-7)	0.547
Last AST (IU/L)	62 (18-82)	29 (24-33)	0.341
Last ALT (IU/L)	49 (13-103)	12 (8-29)	0.401
Last bilirubin (mg/dl)	1.0 (0.6-1.0)	0.8 (0.8-0.9)	0.346
Anti-HB core positive	1/4 (20/80)	2/2 (50/50)	0.343
Comorbidities (Y/N)			
-Dyslipidemias *n* (%)	2/3 (40/60)	1/3 (25/75)	0.635
-Hypertension *n* (%)	3/2 (60/40)	3/1 (75/25)	0.740
-Diabetes *n* (%)	0/5 (0/100)	1/3 (25/75)	0.236
Cause of death			
-CVA	3 (60)	3 (75)	0.635
-Cardiac arrest	1 (20)	0 (0)	0.151
-Anoxia	1 (20)	0 (0)	0.151
-Trauma	0 (0)	1 (25)	0.236
DCD type 2 (*n*)	1/4	0/4	0.343
No-flow time (min)	20	-	
Low-flow time (min)	126	-	
Reasons for discard *n* (%)			
-Necrosis >10%	2 (40)	2 (50)	0.764
-Macrosteatosis >30%	1 (20)	1 (25)	0.858
-Stage 3 fibrosis	2 (40)	1 (25)	0.635
CIT (min)	850 (634-951)	595 (445-799)	0.145
Bile production (>2 ml)	2 (40)	1 (25)	0.635

Abbreviations: ALT, alanine aminotransferase; AST, aspartate aminotransferase; BMI, body mass index; CVA, cerebrovascular accident; DCD, donation after circulatory death; F, female; HB, hepatitis B ICU, intensive care unit; M, male; n, number. Data are expressed as median (interquartile range) or *n* (%).

Cerium oxide nanoparticles administration during machine perfusion of discarded human livers: a pilot study

Authors

Serena Del Turco[1*], Valentina Cappello[2], Christos Tapeinos[3], Aldo Moscardini[4], Laura Sabatino[1], Matteo Battaglini[3], Fabio Melandro[5], Francesco Torri[5], Caterina Martinelli[5], Serena Babboni[1], Beatrice Silvestrini[6], Riccardo Morganti[7], Mauro Gemmi[2], Paolo De Simone[5], Paulo N. Martins[8], Laura Crocetti[6], Adriano Peris[9], Giuseppina Basta[1], Gianni Ciofani[3] and Davide Ghinolfi[5*].

Table of contents:

Supplementary Material and Methods

NMP setup description

The NMP consisted of a centrifuge pump (S5, LivaNova-GmbH, München, Germany), a liver perfusion circuit (SorinGroup, Mirandola, Italy) with a bifurcation after the pump to provide blood flow to the portal vein and the hepatic artery, a cardiotomy reservoir, a heater (Thermic Generator System3T, LivaNova-GmhB, Munchen, Germany), and an institutionally developed organ receptacle. A C-clamp was employed on the tubing to portal infusion after bifurcation to manage portal and arterial flows. A blood-based perfusate, supplemented with colloid solution (Gelofusine®, Braun, Melsungen, Germany) (1000ml), human albumin 200 g/L (Albital®, Kedrion, Barga, Italy) (100 ml), Cefazoline (Teva Italia, Milan, Italy) (1000 mg), Heparin 25,000 units (Epsoclar®, Hospira Italy, Naples, Italy), sodium bicarbonate 8.4% solution (Monico, Venice, Italy) (30ml) and the required volume of normal saline to reach a total volume of 2.0 L, was used for graft perfusion. Packet red blood cells units were added to maintain a hematocrit level between 9-12. The outflow was drained via the intrahepatic and suprahepatic vena cava freely in the organ receptacle and recirculated. Oxygen flow (30% FiO2) was started at 2 L/min through the oxygenator integrated in each circuit and then adjusted to maintain the infusion oxygen pressure at around 200-250 mmHg. Blood gas analysis was evaluated every 30 minutes to adjust ionogram, pH and oxygen pressure. Vascular flows and pressures were continuously monitored. Pressures range targets were 5-8 mmHg for the portal vein and 70-90 mmHg for the hepatic artery. Perfusate alanine and aspartate-aminotransferases, glucose and lactate levels were measured every hour.

Synthesis and characterization of Alb-NC preparation.

a) Synthesis of Alb-NC

A sterile aqueous dispersion of commercial nanoceria (20 mg/ml) (2ml volume) (5 nm, Cerium (IV) oxide, Alfa Aesar, Ward Hill, MA, USA) was placed under sonication (ampl. 50%) at 4ºC, while a sterile DPBS (Sigma-Aldrich, St. Louis, MO, USA) solution of albumin (1 mg/ml), was added drop-

by-drop (2 ml volume). After albumin addition, the mixture was sonicated for 30 minutes and subsequently stirred vigorously for 3 hours at the same temperature. Alb-NC were cleaned thrice with sterile water to remove the unconjugated components using filtration centrifugation (Amicon filters, MWCO~100 kDa) at 7500xg. After each centrifugation, the concentrated sample in the apical part was re-dispersed in water by vigorous pipetting or slight tip sonication for a few seconds. After cleaning, the samples were re-dispersed in sterile water at concentrations 8-10 mg/ml and stored at 4℃ until further use.

b) Morphological characterization of Alb-NC

The morphology of the Alb-NC was performed using a FEI 200 scanning electron microscope (SEM) and a Zeiss Libra 120 + transmission electron microscope (TEM).

For SEM, the operating voltage ranged from 5–20 keV, with beam currents varying from 0.17 nA to 43 pA. The samples were diluted at 100 μg/mL and were subsequently cast (20 μL volume) on electron microscopy stubs covered with aluminum foil. The samples were left to dry overnight. Before analysis, the samples were coated with gold at 25 mA for 70 s.

For TEM, the operating voltage was 120 keV. The instrument was equipped with an in-column omega filter for energy-filtered imaging. The samples, at various dilutions, were sonicated for a few seconds and were cast on 300 mesh carbon-coated copper grids.

c) Stability of Alb-NC

Dynamic light scattering studies were carried out to assess the stability of the Alb-NC, using a Zetasizer Nano ZS90 (Malvern Panalytical). The samples were dispersed at a concentration of 100 μg/mL and a final volume of 1 mL and were sonicated for 1 minute using a tip sonicator (ampl. 50%) before the first measurement (t=0). Afterward, the samples were kept at 4 °C for the whole duration of the experiment (25 days). The temperature measurement was set at 25 °C. Before each measurement, the samples were left for 5 minutes at room temperature to equilibrate. The number of measurements for each sample was set at three, the number of runs at ten, and the duration of each run was set at ten seconds.

d) Surface analysis Alb-NC by X-ray photoelectron spectroscopy (XPS)

The XPS measurements were carried out with a Kratos Axis Ultra^{DLD} spectrometer (Kratos Analytical Ltd., UK) using a monochromatic Al Kα source (hν = 1486.6 eV), operated at 20 mA and 15 kV. The high-resolution Ce 3d spectrum was collected at pass-energy of 20 eV and energy step of 0.1 eV. The Kratos charge neutralizer system was used during data acquisition. The spectra were analyzed with CasaXPS software (Casa Software, Ltd., version 2.3.24). The sample was prepared by drop-casting of few microliters of a concentrated solution of CeO_2 into a highly oriented pyrolytic graphite (HOPG) substrate.

TEM analysis

Tru-cut biopsies at T0 and T1 were twice washed in PBS and immediately posed in the fixative solution (Glutaraldehyde 0.5% + Paraformaldehyde 4% in PBS). Four hours later samples were rinsed in PBS and stored at 4°C in 0.4% Na Azide in PBS till further processing as described elsewhere [1]. Briefly samples were divided in small blocks of 1 mm cube and fixed again in 2% glutaraldehyde in Cacodylate buffer 0.1M pH 7.4, then washed and postfixed in reduced osmium tetroxide (1% OsO4 + 1% K3Fe(CN)6 in Cacodylate buffer 0.1M). After washing samples were stained with pure X solution [2] and finally dehydrated in a gradient series of ethanol/water. Processed samples were then embedded in epoxy resins and backed for 48 hours at 60°C. Tissue embedded samples were then sectioned at room temperature, using an ultramicrotome (UC7 - Leica Microsystems, Vienna, Austria). A 35° diamond knife (DiATOME, Nidau, Switzerland), with a large cutting window (50 nm- 1 um) has been used for both thicker and thinner sections.

For each sample an array of about 60 microns has been collected as follows:

1) 20 sections for light microscopy (500 nm each one)
2) 18-30 sections for EM (3 grids – 90 nm each one)
3) 20 sections for light microscopy (500 nm)
4) 18-30 sections for EM (3 grids – 90 nm)
5) 20 sections for light microscopy (500 nm)

6) 18-30 sections for EM (3 grids – 90 nm)
7) 20 sections for light microscopy (500 nm)
8) 18-30 sections for EM (3 grids – 90 nm)
9) 20 sections for light microscopy (500 nm)

Number of sections for each grid can be changed due to sample size between 6 to 10 sections. 500 nm thick sections were stained with conventional histological staining solution (0.1% methylene blue and 0.1% toluidine blue in phosphate buffer 240 mM pH 7.4) and imaged with an optical microscope (DM750, Leica Microsystem, Vienna, Austria), equipped with an ICC50HD (Leica Microsystem, Vienna, Austria) digital camera. We used 10X HI PLAN (NA = 0.25) objective (Leica Microsystem, Vienna, Austria (**Supplementary Fig. 1A)).** The first grid after light microscopy recording has been analyzed in Low Mag mode (200X-250X) using a Zeiss Libra 120 Plus transmission electron microscope, operating at 120 kV and equipped with an in-column omega filter for the energy filtered imaging (Zeiss, Oberkichen, Germany – **Supplementary Fig. 1B,C**). The fine architecture of cells and tissue have been imaged in Mag Mode at the magnification scale between 4000 X and 40000 X.

a) Morphometric Maths: Evaluation of Lipid Droplets (LD) peroxidation

For each section we only selected those 200X LM micrograph in which more than 4 hepatocytes were clearly visible. Then we manually counted all the peroxidated LD (those ones with a pale halo between membrane and lipid content) and we evaluated the ratio between those structures and the whole number of LD (both normal and peroxidated).

For each sample we analyzed between 20 to 35 meshes and we used these values for the statistical analysis and reported as average, standard deviation, number, and statistical significance.

The total number of LD is drastically influenced by the steatosis level of the organ, so we preferred to consider only the ratio between the two classes of lipid droplets instead then their numerosity.

b) *Morphometric Maths: Evaluation of size and number of lipofuscin granules*

For the evaluation of lipofuscin granules, we used 10 micrographs, randomly imaged in Low Magnification mode (250X), for each sample. For each mesh we measured the total tissue surface (subtracting empty resin and vessel lumen) for normalizing our values respect the real hepatocytes area. The area of lipofuscin granules has been calculated using NIH ImageJ 1.53 software, while the number has been counted manually. Both these values have been normalized for the total tissue surface.

Inductively coupled Plasma-Mass spectrometry Analyses

The liver biopsies were dried for about 8h at 80°C until constant weight was obtained. The dried samples were digested in 2 mL of freshly made aqua regia overnight at 120°C, if necessary more aqua regia was added. The perfusates were weighed and digested without drying. After the digestion, every sample was dried and re-suspended in 6 mL of a 3% nitric acid solution. All solutions were purchased from Merck with Suprapure purity (for trace analysis). The amounts of cerium were determined after analysis on a ICP-MS Agilent 7700, using standard calibration curves obtained from a Multielement standard solution for ICP (Sigma-Aldrich). The Ce content was normalized in ng/mg of dried sample for the liver biopsies while for the perfusates the Ce content was normalized in ng/mg of fresh sample (not dried).

Telomere Length and mtDNA4977 Deletion Measurement

DNA was extracted from <25 mg of liver tissue sample by Quick-DNA Miniprep kit (Zimo Research, Orange, CA, USA), following manufacturer's instructions.

a) Relative Telomere Length (TL) was assessed by Monochrome Multiplex Quantitative PCR (MMQPCR) according with the method described previously [3] with some modifications. MMQPCR was carried out into a 384-well CFX RT-PCR Bio-Rad System in a 10 mL reaction mix containing 20-50 ng of genomic DNA in Bio-Rad iQ SYBR Green Supermix. Forward and reverse primer sequences for telomere and b-globin gene (S) and the thermal profile and cycling program have been previously reported [3,4]. Each sample was assayed in duplicates, with negative and positive controls

included. A standard curve for telomere and S was also evaluated in each assay as control of amplification efficiency and linearity (starting from 125 ng in a 4-fold dilution).

b) Relative quantification of mtDNA4977 bp deletion by Real Time PCR

The mtDNA4977 deletion content was measured by Real Time PCR amplification in 10 mL of reaction containing 20-50 ng of DNA. ND1 gene in undeleted region of mitDNA was used as reference, the remaining fragment after 4799-bp deletion of mitDNA (mitDNA^{4977}) was the internal marker of the occurred deletion, and beta-globin gene was the reference gene for genomic DNA normalization. The primers were obtained from the literature [5] and Real Time assays were performed in duplicates in a Bio-Rad 384 CFX System, for 40 cycles of amplification (95°C for 5 sec., 60°C for 10 sec.). Bio-Rad SsoAdvanced Universal Sybr Green Supermix was used for the reaction. The efficiency of the Real Time PCR reaction was evaluated by calibration curves, included in each experimental plate for each gene evaluated (starting from 125 ng in a 4-fold dilution). Curves with R^2>0.95 were considered acceptable.

In vitro study

a) WRL68 cell culture. The human WRL68 normal hepatocyte cell line (Sigma-Aldrich, St. Louis, MO, USA) was cultured in Eagle's Minimal Essential Medium (EMEM) (Sigma-Aldrich) containing 1% non-essential amino acids, 10% fetal calf serum (FCS) (Life Technologies, Carlsbad, CA) and penicillin/streptomycin.

b) Viability assay. Wst-1 assay was performed after 4-24 h of Alb-NC treatment at 50 µg/mL as previously described [6].

c) TEM. Hepatocytes were fixed as monolayer with 2% glutaraldehyde solution in Cacodylate buffer 0.1M, then scraped, spun (13.200 rpm), and treated as cells' pellet following the same protocol used for tissue starting at 2% glutaraldehyde step. Cell's pellet was sectioned in 90 nm thick sections and directly collected on 300 mesh copper grids for the ultrastructural analysis of NC uptake, cells were treated as previously described [7].

d) Intracellular ROS detection. The antioxidant activity of Alb-NC was tested in WRL-68 activated by 2 h of treatment with H_2O_2 (150 μmol/L) and then treated with Alb-NC for 4 h. Intracellular ROS generation was assessed as previously described [6].

References

1. Cappello, V, Vezzoli, E, Righi, M, Fossati, M, Mariotti, R, Crespi, A, et al. Analysis of neuromuscular junctions and effects of anabolic steroid administration in the SOD1G93A mouse model of ALS. *Mol Cell Neurosci*. 2012;51(1-2):12-21. doi:10.1016/j.mcn.2012.07.003.
2. Moscardini, A, Di Pietro, S, Signore, G, Parlanti, P, Santi, M, Gemmi, M, et al. Uranium-free X solution: a new generation contrast agent for biological samples ultrastructure. *Sci Rep*. 2020;10(1):11540. doi:10.1038/s41598-020-68405-4.
3. Cawthon, RM. Telomere length measurement by a novel monochrome multiplex quantitative PCR method. *Nucleic Acids Res*. 2009;37(3):e21. doi:10.1093/nar/gkn1027.
4. Sabatino, L, Botto, N, Borghini, A, Turchi, S, Andreassi, MG. Development of a new multiplex quantitative real-time PCR assay for the detection of the mtDNA(4977) deletion in coronary artery disease patients: a link with telomere shortening. *Environ Mol Mutagen*. 2013;54(5):299-307. doi:10.1002/em.21783.
5. Baykara, O, Sahin, SK, Akbas, F, Guven, M, Onaran, I. The effects of mitochondrial DNA deletion and copy number variations on different exercise intensities in highly trained swimmers. *Cell Mol Biol (Noisy-le-grand)*. 2016;62(12):109-115. doi:10.14715/cmb/2016.62.12.19.
6. Cervelli, T, Panetta, D, Navarra, T, Andreassi, MG, Basta, G, Galli, A, et al. Effects of single and fractionated low-dose irradiation on vascular endothelial cells. *Atherosclerosis*. 2014;235(2):510-518. doi:10.1016/j.atherosclerosis.2014.05.932.
7. Del Turco, S, Ciofani, G, Cappello, V, Gemmi, M, Cervelli, T, Saponaro, C, et al. Cytocompatibility evaluation of glycol-chitosan coated boron nitride nanotubes in human endothelial cells. *Colloids Surf B Biointerfaces*. 2013;111:142-149. doi:10.1016/j.colsurfb.2013.05.031.
8. Zhou, YH, Perket, JM, Zhou, J. Growth of Pt Nanoparticles on Reducible CeO2(111) Thin Films: Effect of Nanostructures and Redox Properties of Ceria. *Journal of Physical Chemistry C*. 2010;114(27):11853-11860. doi:10.1021/jp1007279.
9. Beche, E, Charvin, P, Perarnau, D, Abanades, S, Flamant, G. Ce 3d XPS investigation of cerium oxides and mixed cerium oxide (CexTiyOz). *Surface and Interface Analysis*. 2008;40(3-4):264-267. doi:10.1002/sia.2686.

Legend to Supplementary Figures

Supplementary Figure 1. Tissue maps generation. Representative images of maps generation, a) light microscopy images, of the whole section, were collected 10X objective; b) representative scheme of Low Magnification EM micrographs maps; c) partial maps build up with some of the showed micrographs.

Supplementary Figure 2 ALT, AST, lactate, pH and vascular flow variation during NMP

Supplementary Figure 3A) Scanning electron microscopy of dried NC and albumin combination (Alb-NC): the conjugates result irregular in terms of size and morphology. B) high magnification transmission electron microscopy images showing the Alb-NC conjugates: formation of some fibrils structure is clearly observable. C) Graph demonstrating the Alb-NC's colloidal stability in aqueous medium: the Alb-NC conjugates present an average hydrodynamic diameter (Rd) size of 196.0±5.8nm that remains stable over of 25 days, the whole period in which the stability measurements were carried out. This stability could be attributed to steric hindrances between the fibrous Alb-NC conjugates and potentially weak electrostatic repulsions due to a surface charge of -11.8 ± 1.4 mV. The data were acquired using a zetasizer nano ZS and plotted using OriginPro 9.1. D) XPS graph of the Alb-NC conjugates showing the energy peaks typical for Ce 3d, and related outcome of the fitting procedure. The best fit was obtained with five sets of spin-orbit split doublets, three of which correspond to Ce(IV) (dark red profiles), and two to Ce(III) oxides (green profiles), data which are in agreement with the work of Zhou et al. [8]. The splitting between the two components of each doublet was set to 18.6 eV, as reported by Bêche et al. [9] where the intensity ratio between the two components was set to 3:2, due to spin-orbit coupling. The relative atomic concentration of Ce(III) and Ce(IV) ions in the sample was calculated from the ratio of the sum of the integrated areas of the XPS 3d peaks related to Ce(III) and Ce(IV) of the total integral area for the whole Ce 3d region, resulting in Ce(III) 69±2 %, Ce(IV) 31±2 %, corresponding to a Ce(III)/Ce(IV) ratio of ~2.2.

Supplementary Figure 4 Representative EM micrographs of livers of control group (upper line) and study group (middle and bottom lines) at T0 and T1. Alteration of matrix (**a, d,g**, white boxes) and cristae (d**, g**) and the presence of giant mitochondria (GM) (**d**) at T0. In control group, mitochondrial pool undergoes alteration moving from T0 to T1 and we observed pale and/or swollen mitochondria with disorganized inner cristae (* labels disorganized inner cristae), b) and as well as, in several cases,

the presence of giant mitochondria (GM) (c). Livers of study group showed a morphological improvement of the mitochondrial pool at T1 (e,h). Small Alb-NC aggregates that for their localization, shape, and size could be in the top of mitochondrial cristae (f,i) as shown in the higher magnification of the boxed regions (f and i, arrow heads). Scale bar: 500 nm (a, b, c, d, e, g, h), 100 nm (f, i).

Supplementary Figure 5 (A) TEM images of WRL68 untreated (a), treated with H_2O_2 (150 μmol/L) for 4 h (b), with NC alone (50 μg/mL) for 4 h (c) and after treatment with of H_2O_2 (d). Untreated or Alb-NC- treated cells show similar cellular morphology with cells in mitosis (M). A different distribution of chromatin was noted in in the nuclear compartment (white arrows) of H_2O_2-treated cells (b) compared with untreated cells (a, black arrow). The boxes at the bottom left of each panel show the ultrastructure of mitochondria. Mitochondria are small with very organized inner cristae and a quite electron dense matrix in a and c panels (§ in c labels an aggregate of Alb-NC), while swollen mitochondria, with disorganized cristae and pale matrix are observed in stressed cells (b). After treatment with Alb-NC we noted a rescue of mitochondrial phenotype (d). Highlighted by arrowheads in (d) some NC escaped from the endosomes. **(B**) Cell viability assessment of WRL-68 untreated or treated with Alb-NC (50 μg/mL. for 4-24 h, evaluated by WST-1 assay. Data are expressed as mean ± SD of optical density arbitrary units (AUs) at 405 nm, and are representative of three independent experiments **(C)** Quantitative evaluation of ROS levels performed in H_2O_2-treted cells in presence or absence of Alb-NC (50 μg/mL). Data are expressed as mean ± SD of optical density arbitrary units (AUs). Data are expressed as mean ± SD of fluorescence arbitrary units. *$p < 0.05$ versus H_2O_2-treated cells.

Supplementary Figure 6 Cytokine release in perfusates**.** The fold change release of cytokines and chemokines in perfusate of the control and study group. Data are expressed are expressed as mean fold change ± SEM calculated as ratio of (final value at T1 - initial value at T0)/(initial Value at T0).

Figures

Supplementary Figure 1

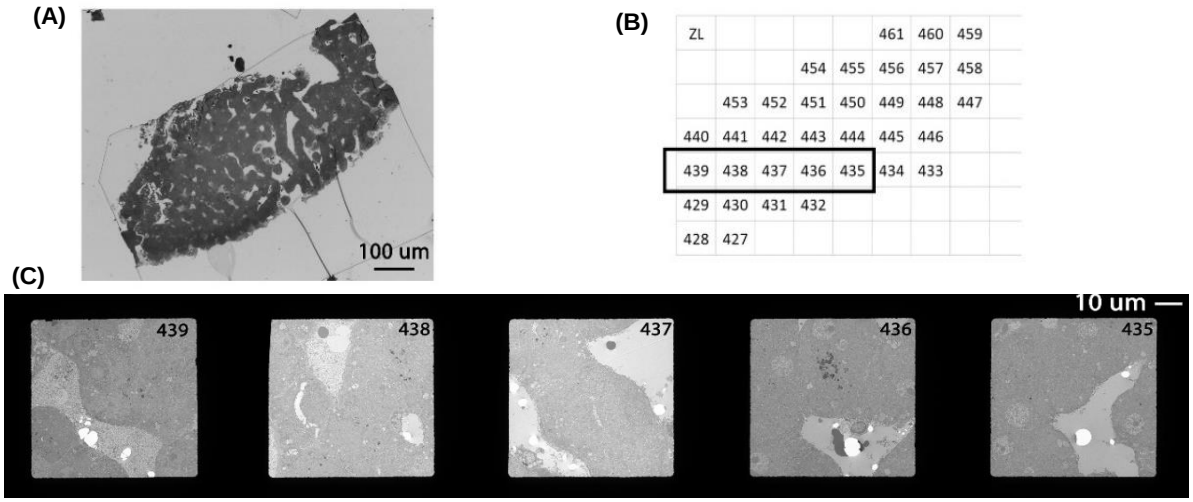

Supplementary Figure 2

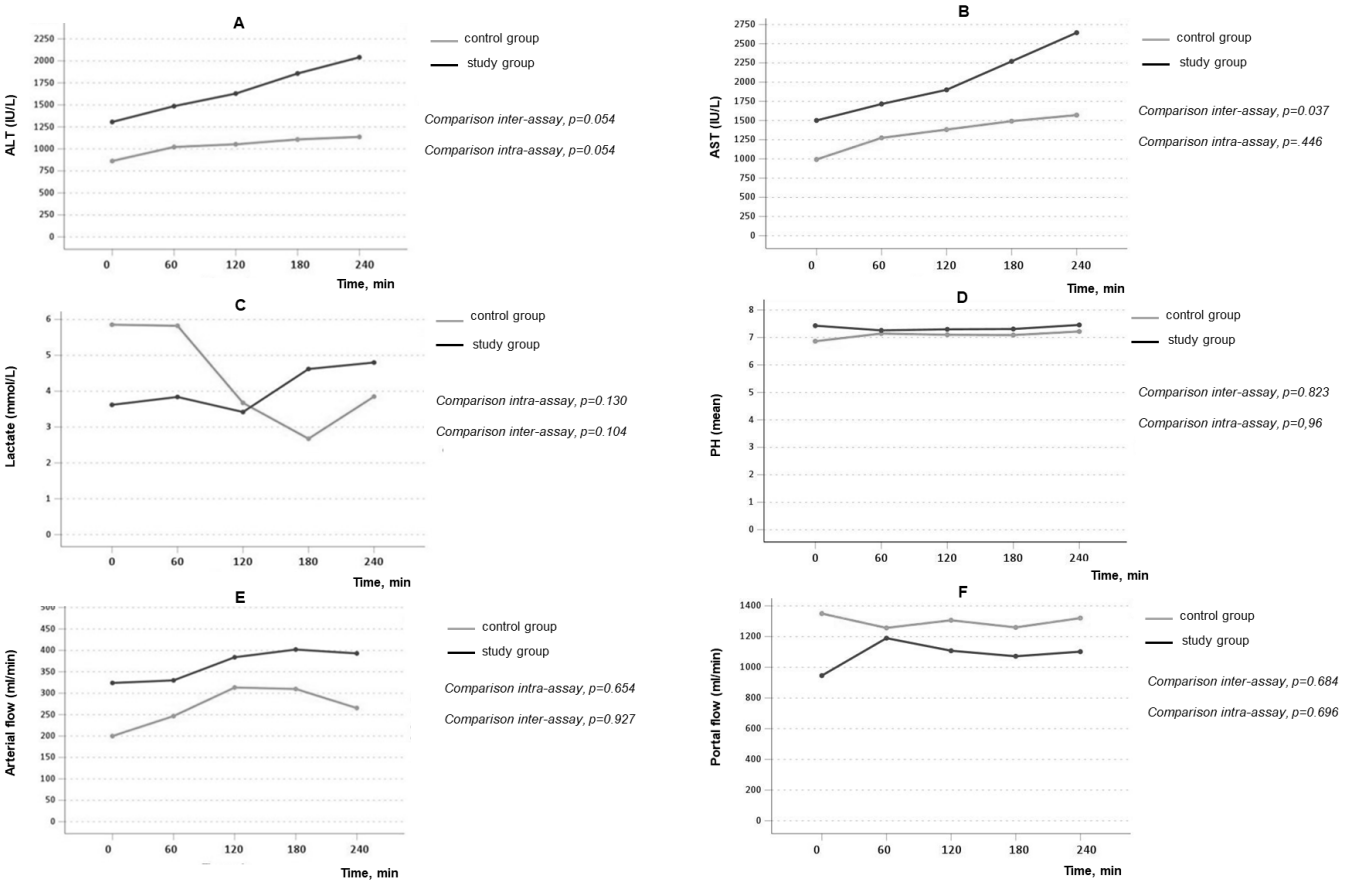

Supplementary Figure 3

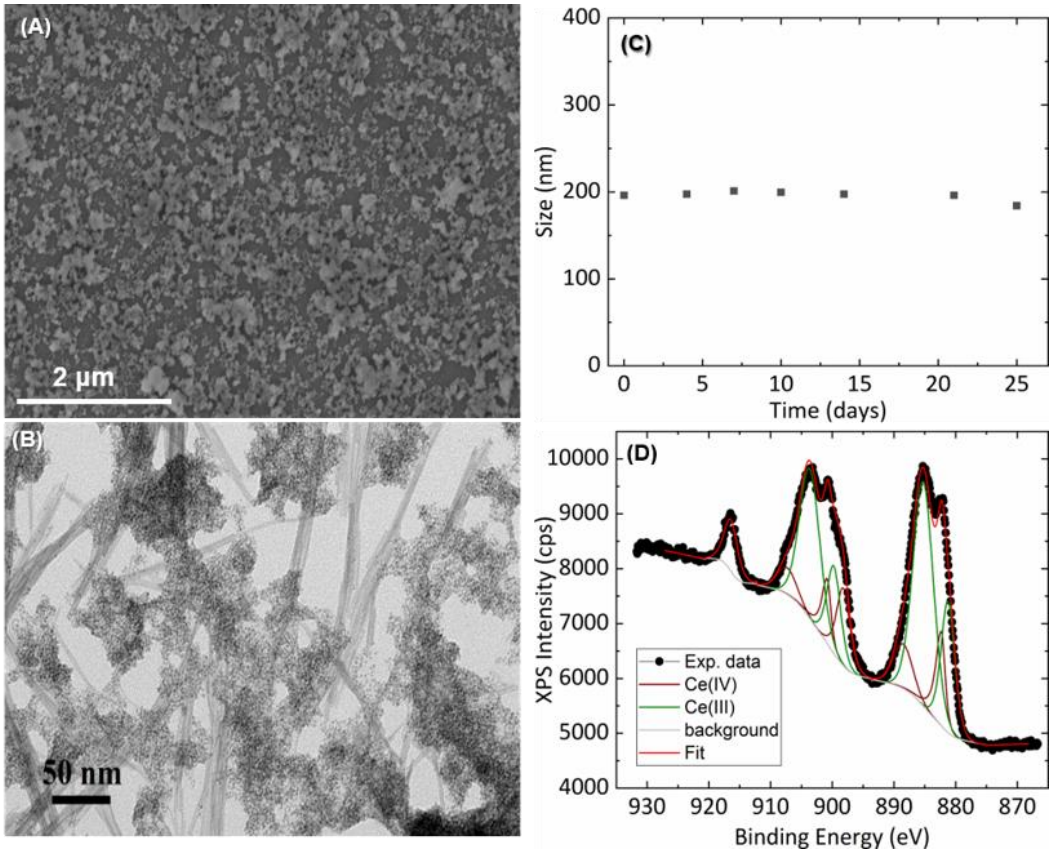

Supplementary Figure 4

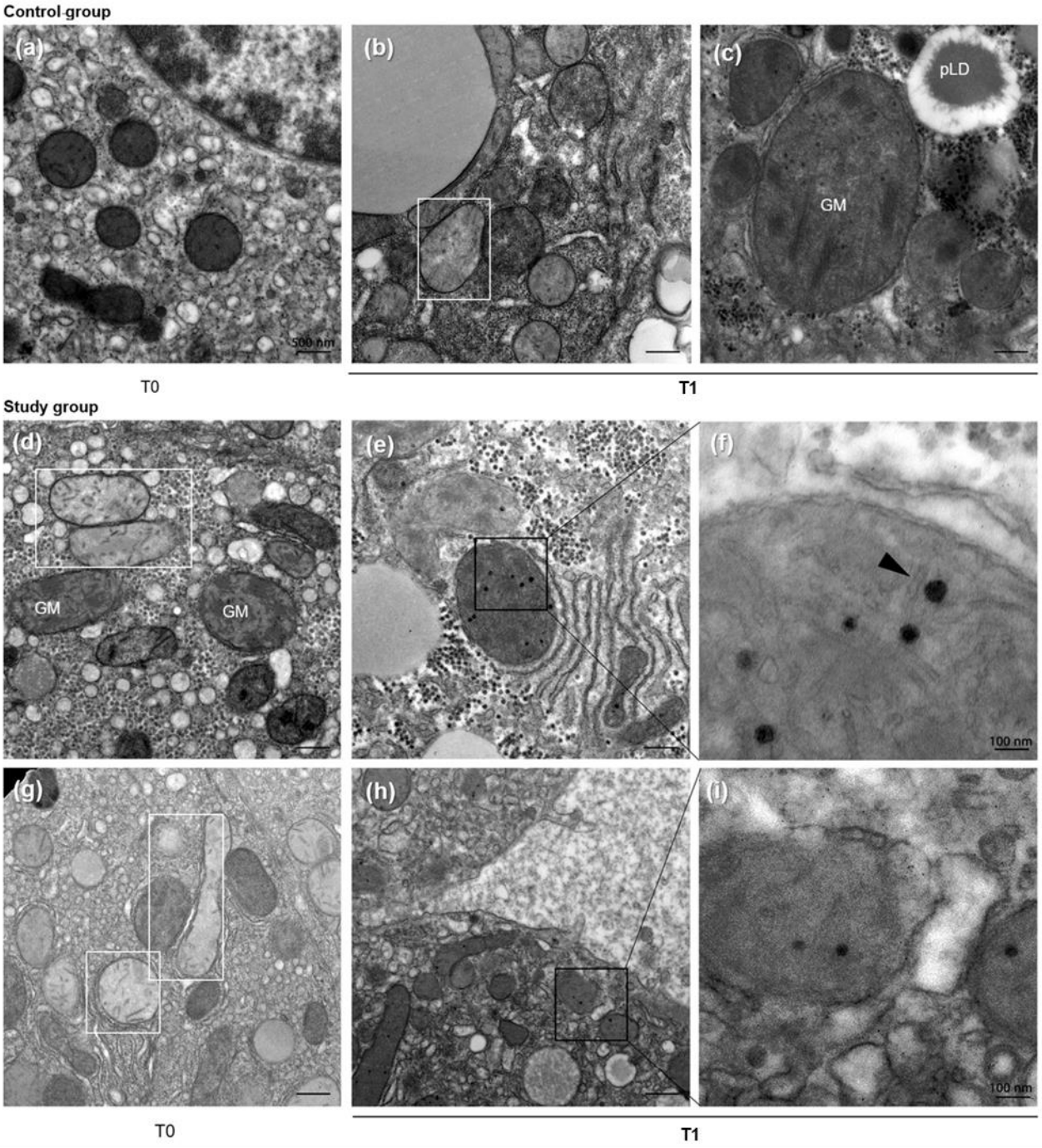

Supplementary Figure 5

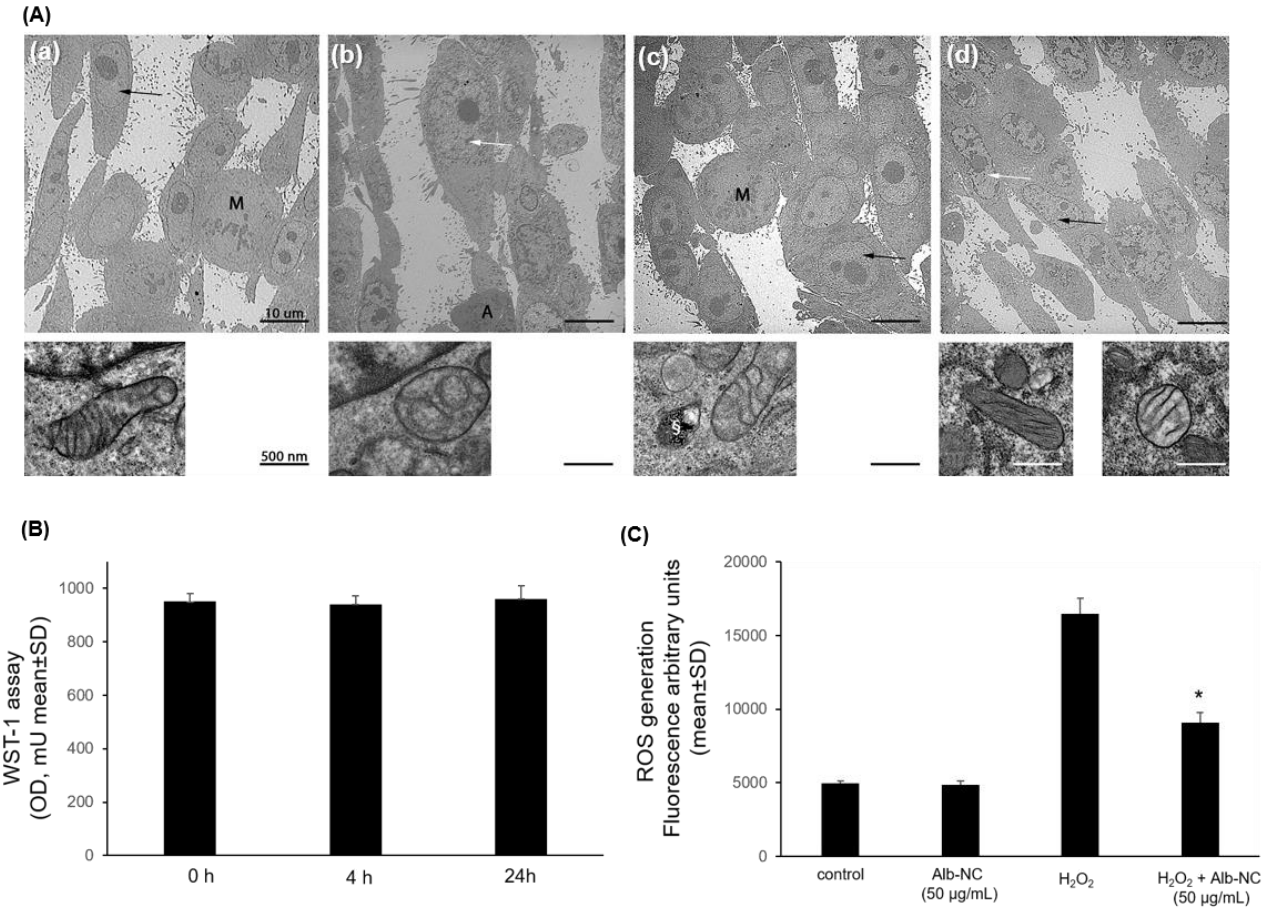

Supplementary Figure 6